Artesunate pErk up HepG2 cells to die through apoptosis *in vitro*

Johnny Kuan-Un Wong *[,1], Sophie Ling Shi *[,1], Haitao Wang [1], Fuqiang Xing [1], Yingyao Quan [1], Kristy Hio-Meng Wong [2], Ada Hang-Heng Wong #[,1], Chuxia Deng #[,1]

[1] Cancer Centre, Faculty of Health Sciences, University of Macau, Macau S.A.R., China.

[2] Summer Program for Secondary School Students, Faculty of Health Sciences, University of Macau, Macau S.A.R., China.

Correspondence: adahhwong@um.edu.mo (A.H.W.), cxdeng@um.edu.mo (C.D.)

Abstract

Artesunate is a chemical derivative of Artemisinin that was reported to combat cancer. In this study, screening of eleven cancer cell lines from six tissue origins demonstrated that Artesunate effectively inhibited proliferation of liver cancer cell lines *in vitro*. Using HepG2 cells as a model, Artesunate induced Erk1/2 phosphorylation and DAPK1 dephosphorylation, triggering apoptosis. Complementation with U0126 revoked Erk1/2-DAPK1 phosphorylation and exerted modest proliferative advantage at early time points, but eventually did not rescue HepG2 cells from death. U0126 induced multiploid formation independent of Artesunate, resulting in cell cycle arrest within 24 h post-treatment. However, Artesunate was ineffective in inhibiting tumor growth *in vivo*. Prevailing evidence manifested that tissue architecture did not confer to Artesunate inefficacy *in vivo*. Hence, we hypothesized that the rapid blood clearance of Artesunate attributed to its inefficacy *in vivo*. Given that Artesunate had no apparent impact on mouse body weight and blood biochemistry, Artesunate provided an option for chemotherapy with mild side effects, if smart design of drug delivery might improve its distribution *in vivo*.

Keywords: Artemisinin, Artesunate, liver cancer, apoptosis, Erk

Introduction

Liver cancer is ranked third on the mortality cancer list in China [1] and worldwide. Hepatocellular carcinoma (HCC) is the most common form of liver cancer. Physical treatment of liver cancer includes hepatectomy, embolization and external beam radiation therapy (EBRT), whereas chemical treatment includes chemotherapy, targeted therapy and immunotherapy [2]. Patients undergoing cancer therapy not only suffer from the disease, but also suffer from the side effects, especially nausea, hair loss, *etc*, due to radiotherapy or chemotherapy. Hence, the search for effective cancer treatment and/or prevention method becomes imperative.

Traditional Chinese Medicine (TCM) is generally considered to exert low cytotoxicity and mild side effects. However, the chemical complexity of herbal and animal extracts led to poor administration guidelines, inconsistency of medicinal dose(s), and unclear exemplification of pharmacological mechanism(s). Hence, the application of TCM in Precision Medicine seemed vain.

Artesunate is a chemical derivative of Artemisinin. Artemisinin is a natural compound extracted from the herb *Artemisia annua* to combat malaria in TCM [3]. Artemisinin was first discovered by Professor Youyou Tu [3], who was honored half of Nobel Prize in Physiology or Medicine in 2015 for this discovery. Since then, the mode of action of this drug and its derivatives were studied and applied to other purposes, for example, Alzheimer's disease [4], virus infections [5] and cancer [6-10]. Artemisinin and Artesunate underwent Phase I clinical trial to treat solid tumors caused by human papillomavirus.

Artemisinin was reported to kill cancer cells by carbon-centered radicals generated by its endoperoxide bridge, the pathway of which was catalyzed by intracellular iron [8]. Artesunate, as a derivative of Artemisinin, was predicted to exert similar effects. However, this study showed that Artesunate did not induce apoptosis due to high intracellular iron in the liver cancer cell line HepG2. In fact, screening of a total of eleven cancer cell lines prevailed that there was little correlation between intracellular iron and drug susceptibility. Instead, results showed that the Erk1/2-DAPK1 pathway was activated to trigger apoptosis *in vitro*.

Results

Artesunate inhibited HepG2 cell proliferation and activated Erk1/2-DAPK1 pathway to promote apoptosis *in vitro*.

In this study, we screened eleven cancer cell lines belonging to six tissue origins against Artemisinin and its three derivatives, namely Artesunate, Dihydroartemisinin and Artemether. Results showed that Artesunate was the most potent Artemisinin analog *in vitro* (Figure 1A). Moreover, the hepatocellular carcinoma (HCC) cancer cell line HepG2 was susceptible to all four analogs (Figure 1B). However, we did not see significant cell cycle arrest in HepG2 cells treated with 30 μM Artesunate as compared to control at 12 h post-treatment (Figure 1C), suggesting that Artesunate did not trigger cell cycle arrest to inhibit HepG2 cell proliferation as reported in other cell lines [7, 9]. Additionally, even though liver is rich in iron (Figure 1D), HepG2 cells contained the lowest intracellular iron among all liver cancer cell lines tested in this study (Figure 1E), suggesting that radical oxygen species (ROS) generated from the catalysis of intracellular iron on Artemisinin and its analogs [8] did not confer to HepG2 susceptibility towards Artesunate. Furthermore, ROS staining did not show significant increase in HepG2 cells treated with any of the four Artemisinin analogs at 12 h post-treatment (Figure 1F), in consistence with the low intracellular iron in HepG2 cells (Figure 1A and 1E). Consistently, there was no significant pH changes in HepG2 cells after 12 h treatment with 30 μM Artesunate as compared to control (Figure 1G). Taken together, our results depicted that Artesunate inhibited HepG2 cell proliferation without compliance to known Artemisinin modes of action.

In order to decipher the mechanism of action of Artesunate on HepG2 cells, we tested the phosphorylation of three kinases, namely Erk1/2, p38 and AMPKα after adding 30 μM Artesunate to HepG2 cells by Western blotting. Western blot analysis showed that the ratio of phosphorylated Erk1/2 slightly increased at 10 min after Artesunate addition as compared to control, followed by reduced phosphorylation after 30 min post-treatment (Figure 2A). On the other hand, increased phosphorylated p38 was observed at 10 min post-treatment in control and in HepG2 cells treated with Artesunate (Figure 2A). No AMPKα phosphorylation was

observed in control and under Artesunate treatment (Figure 2A). Hence, we deduced that Erk signaling was involved in HepG2 cell killing by Artesunate.

Erk1/2 phosphorylation is predominantly known to promote cell proliferation. However, death-associated protein kinase 1 (DAPK1) was reported to be phosphorylated by Erk1/2 at Ser735, leading to apoptosis [11]. DAPK1 is a multi-domain protein kinase (Figure 2B), involved in various processes including apoptosis and autophagy [12]. However, because no commercial antibody against DAPK1-pSer735 was available, so we tested the inhibitory phosphorylation site on Ser308, which was reported to be crucial for its kinase activity [13, 14]. We hypothesized that DAPK1-pSer308 was dephosphorylated upon Erk1/2 activation by Artesunate treatment. Western blot analysis showed that DAPK1-pSer308 was partially dephosphorylated between 30 min and 1 h after addition of 30 μM Artesunate (Figure 2C). Dephosphorylation of DAPK1 coincided with phosphorylation of Erk1/2 between 10 min and 30 min post-treatment (Figure 2C), supporting for our hypothesis that Artesunate induced Erk1/2 phosphorylation and subsequent DAPK1 dephosphorylation.

U0126 is a specific inhibitor of MEK1, an upstream kinase that phosphorylates and activates Erk1/2 [15]. U0126 was used to suppress Erk1/2 phosphorylation induced by Artesunate treatment (Supplementary Figure 1A). While Artesunate enhanced Erk1/2 phosphorylation at 10-30 min post-treatment, addition of U0126 reduced Erk1/2 phosphorylation and total protein after 1 h post-treatment in the absence and presence of Artesunate treatment (Figure 2C). Dephosphorylation of DAPK1 was abolished in HepG2 cells treated with Artesunate and U0126 (Figure 2C), supporting for Erk1/2-mediated DAPK1 dephosphorylation.

Next, we asked for the cell death mechanism of Artesunate treatment. Western blot analysis showed that Caspase-3 was enhanced after 6 h of Artesunate treatment, whereas Beclin-1 and LC3B did not show significant difference as compared to control after Artesunate treatment (Figure 2D). Measurement of caspase activity by Caspase-Glo® assay showed increased caspase activity in HepG2 cells after 6 h treatment with Artesunate, the activity of which peaked at 12 h post-treatment and declined afterwards (Figure 2E), possibly due to retarded cell proliferation and cell death (Figure 2F). Indeed, cell proliferation was slowest in Artesunate-treated HepG2 cells (Figure 2F). In concordance with our hypothesis that Artesunate promoted apoptosis via Erk1/2-DAPK1 pathway, U0126 modestly repressed caspase activity (Figure 2E) and increased confluence (Figure 2F) in HepG2 cells simultaneously treated with Artesunate and U0126. Repression of caspase activity by U0126 under Artesunate treatment was validated using a Sensor C3 fluorescence resonance energy transfer (FRET) reporter system [16] (Supplementary Figure 1D). 24 h time-lapse imaging illustrated an increase in FRET in HepG2 cells treated with Artesunate and U0126 as compared to Artesunate treatment alone (Supplementary Figure 1E), suggesting of diminished Caspase-3 activity in double treated cells. Image analysis of the FRET images showed that Caspase-3 activity gradually increased starting 12 h post-treatment (Supplementary Figure 1F), in consistence to upregulated Caspase-3 protein levels at 6 h post-treatment on Western blot (Figure 2D). To note, U0126 treatment alone also increased caspase activity after 6 h treatment as compared to control (Figure 2E), explaining the modest effect of U0126 on caspase activity in HepG2 cells under double treatment with Artesunate and U0126 (Figure 2E). Furthermore, caspase activity dropped to levels below control after 36 h post-treatment in U0126-treated HepG2 cells (Figure 2E), further supporting for the lack of rescue by double treatment. In double treated cells, U0126 did not rescue HepG2 cells from cell death caused by Artesunate treatment (Figure 2E and 2F).

Decrease of caspase activity to levels below control in Figure 2E was deduced to be caused by cell death, reinforced by images taken during IncuCyte® analysis summarized in Figure 2F. It was noteworthy that the seeding cell density used in this IncuCyte® analysis was 10,000 cells/well on 96-well plate, in compliance to the seeding cell density of the Caspase-Glo® assay necessary for measurement. Hence, over-confluence halted proliferation of control cells after 24 h (Figure 2F).

Furthermore, we observed that Erk1/2 phosphorylation was enhanced at 10 min post-treatment in both control and Artesunate-treated conditions when cell culture medium was replaced during drug addition (Supplementary Figure 1B), whereas enhanced Erk1/2 phosphorylation at 10 min was undetected in control if drugs were directly added to culture medium (Figure 2A and 2C). DAPK1 dephosphorylation remained detectable at 30 min post-treatment in both experimental procedures (Figure 2C and Supplementary Figure 1B), suggesting that changing medium alone enhanced Erk1/2 phosphorylation that could not be passed downstream.

To this point, our results showed that Artesunate induced Erk1/2 phosphorylation, DAPK1 dephosphorylation and Caspase-3 activation in a temporally sequential manner in HepG2 cells *in vitro*. Furthermore, inhibition of Erk1/2 phosphorylation by U0126 abolished DAPK1 dephosphorylation and modestly repressed caspase activity induced by Artesunate treatment. However, U0126 did not rescue HepG2 cells from cell death during Artesunate and U0126 double treatment.

U0126 did not rescue HepG2 cells from Artesunate treatment because U0126 triggered cell multiploidy independent of Artesunate treatment.

To assess cell proliferation, 5,000 cells/well HepG2 cells were seeded on 96-well plate, as opposed to 10,000 cells/well during cell death assessment (Figure 2E and 2F). Firstly, cell proliferation was assayed by Alamar Blue staining. Results showed that addition of 5 μM U0126 stimulated cell growth in HepG2 cells during double treatment with DMSO or Artesunate before 48 h post-treatment (Figure 3A). However, although cell proliferation rate remained high in U0126-treated HepG2 cells, proliferation slowed down in cells double treated with Artesunate and U0126 after 48 h incubation (Figure 3A). Cell proliferation eventually leveled off in double treated cells to reach the same level as compared to Artesunate-treated cells at 72 h post-treatment (Figure 3A). In contrast, U0126 treatment alone led to higher proliferation than control cells until 72 h post-treatment (Figure 3A).

To investigate the growth defect of Artesunate and U0126 double treated cells, we carried out IncuCyte® *in situ* time-lapse imaging and confluence measurement of HepG2 cells under single or double treatment with 30 μM Artesunate and 5 μM U0126 respectively. IncuCyte® analysis showed that HepG2 cells treated with Artesunate alone or in combination with U0126 rapidly reached 50% confluence within 10 h, but cell growth retarded until 74 h post-treatment (Figure 3B). Cell confluence was slightly higher in Artesunate and U0126 double treated cells as compared to Artesunate treatment alone (Figure 3B). Alternatively, DMSO-treated cells in the absence or presence of U0126 continuously proliferate to reach 100% confluence at 74 h post-treatment without significant difference between the two conditions (Figure 3B). Examination of the cell morphology of HepG2 cells prevailed no difference between cells treated with DMSO and U0126 (Figure 3C). However, Artesunate-treated cells lost suppleness, while lamellipodia were present (Figure 3C). In contrast, most of the Artesunate and U0126 double treated cells became round after 48 h post-treatment (Figure 3C).

Although proliferation curves differed between measurements made by Alamar Blue assay (Figure 3A) and IncuCyte® imaging (Figure 3B) at early time points, proliferation of both the U0126 and DMSO treated cells overtook the Artesunate-treated and double treated cells at 48 h post-treatment in both assays, indicating that this time point was critical to loss of rescue by U0126. Cell morphological difference between HepG2 cells treated with Artesunate alone and in combination with U0126 showed that Artesunate treatment caused the loss of lamellipodia before they started to lose suppleness at 10 h post-treatment, whereas cells double treated with Artesunate and U0126 became round but supple until the majority lost suppleness after 48 h post-treatment (Figure 3C). HepG2 cells treated with U0126 showed no difference in comparison to control cells (Figure 3C). These results suggested that: (1) U0126 treatment alone did not affect cell proliferation or morphology on the population level; and (2) U0126 rescued the phenotype of lamellipodium loss in Artesunate-treated cells, but did not rescue them from retarded cell proliferation or cell death.

Because lamellipodium formation is related to actin cytoskeleton, we performed immunofluorescence (IF) staining of HepG2 cells at 12 h post-treatment. Results showed that Artesunate treatment retracted actin from the periphery of cells, whereas double treatment with U0126 rescued this phenotype regardless of medium replacement (Figure 3D and Supplementary Figure 1C).

During morphology analysis, we observed multiploid formation in U0126-treated HepG2 cells, which was seen independent of Artesunate treatment. Because U0126 could not rescue HepG2 cells from death under Artesunate treatment (Figure 3A and 3B), we wondered if this phenomenon could be explained by multiploidy induction by U0126. Examination of over 6,000 centrosome-distinguishable mitotic cells under IF staining for each treatment condition showed that 96.2% of DMSO-treated HepG2 cells underwent diploid mitosis, whereas U0126 resulted in formation of triploids in 20.4% of cells and, to a much lesser extent, multiploids (Figure 3E). In parallel, double treatment with Artesunate and U0126 resulted in 16.8% of triploids (Figure 3E). Artesunate-treated cells showed 8.6% of triploids (Figure 3E), suggesting that no accumulative effect occurred during double treatment. Next, cell cycle analysis by fluorescence activated cell sorting (FACS) demonstrated that the ratio of G2/M to G1/S cells under DMSO treatment increased over the time course from 6 h to 24 h post-treatment (Figure 3F). The percentage of G2/M cells also increased over time in Artesunate- and U0126- treated samples (Figure 3F). However, cell cycle arrest in G1/S phase was observed in HepG2 cells under Artesunate and U0126 double treatment starting at 16 h post-treatment (Figure 3F). The evasion of cell cycle arrest in HepG2 cells under U0126 treatment alone in comparison to double treatment with Artesunate could be explained by the continuous cell turnover in HepG2 cells regardless of insult, as observed in persistent Caspase-3 cleavage (Figure 2D). We hypothesized that the continuous cell turnover assisted HepG2 cells under U0126 single treatment to remove multiploids, so as to remove cells under proliferative adversity. However, in the presence of Artesunate, multiploids independently caused by U0126 could not be efficiently removed, resulting in cell cycle arrest within 24 h post-treatment (Figure 3F). This eventually led to retarded cell proliferation and cell death in double treated cells, seen as the turning point at 48 h post-treatment in cell proliferation assays (Figure 3A and 3B). Collectively, these data provided evidence for the failure of U0126 to rescue HepG2 cells from death under Artesunate treatment.

Taken together, our results prevailed that U0126 inhibition of MEK1-Erk1/2 pathway led to early proliferation advantage in HepG2 cells under Artesunate treatment, but its virtue was eventually overcome by cell multiploidy followed by cell cycle arrest.

Artesunate was ineffective in subcutaneous xenograft mouse model.

We next tested the treatment efficiency of Artesunate in xenograft mouse model. HepG2 cells were subcutaneously implanted into the left and right flank of athymic nude mice (Figure 4A). When tumors grew to 2 mm in any direction, 50 mg/kg Artesunate was intraperitoneally injected to treat the mice. However, tumors continued to grow after Artesunate treatment *in vivo* (Figure 4A). Hematoxylin and eosin (H&E) staining of the xenograft tumors showed that there was no significant difference between control and Artesunate-treated mice (Figure 4A), indicating that Artesunate was ineffective in inhibiting tumor growth *in vivo*.

It is prominent in drug discovery that potent drugs *in vitro* could be ineffective *in vivo*. Since we are engaged in developing *in vitro* drug screening methods for precision cancer therapy [17], we are interested to dissect the dilemma between *in vitro* and *in vivo* drug response. In this pursuit, we studied the HCC biomarkers of α-fetoprotein (AFP) and albumin.

AFP is a liver cancer biomarker elevated in some HCC patients [18]. On the population, though, gene expression of AFP did not significantly differ between human HCC tumor tissue and paired normal tissue (Supplementary Figure 2A), and survival rates did not vary due to different AFP expression (Supplementary Figure 2B). Immunohistochemical (IHC) staining of AFP showed that AFP was lowly expressed in xenograft and untreated livers (Figure 4B). Positive IHC staining of AFP was seen in blood vessels of the xenograft tumors, but not on the epithelial regions in both control and Artesunate-treated mice (Figure 4B). In contrast to *in vivo* results, HepG2 cells expressed AFP on monolayer cultures *in vitro*, with similar expression levels between control and Artesunate-treated cells (Figure 4D). However, AFP expression was compromised in organoid culture *in vitro*, regardless of treatment (Figure 4D), suggesting that AFP expression could be directly regulated by tissue architecture. Additionally, AFP expression was unaffected by Artesunate treatment *in vitro* and *in vivo*. Hence, we deduced that AFP was neither a biomarker nor response indicator in our HepG2 subcutaneous xenograft mouse model.

Albumin is an abundant plasma protein that serves as transportation carrier for many molecules *in vivo* [19]. Albumin was expressed in lower levels in HCC and cholangiocarcinoma tumor tissue than paired normal tissue in humans (Supplementary Figure 2C). Low albumin was correlated to lower survival rate in humans surviving below 70 months after confirmed diagnosis of liver cancer (Supplementary Figure 2D). IHC staining of albumin showed that albumin was similarly abundant in xenograft and untreated mouse livers (Figure 4C), suggesting that the liver function of albumin secretion was unaffected in the subcutaneously engrafted mice. Additionally, Artesunate treatment had no impact on albumin in xenograft livers (Figure 4C). In concert to high albumin in the liver, biochemical analysis of the xenograft mouse blood demonstrated no difference between blood serum albumin in control and Artesunate-treated xenograft mice, whereas the untreated mice without engraftment showed more diverse blood serum albumin levels (Figure 4E), suggesting that albumin secretion became more consistent in xenograft mice. In contrast, albumin was reduced in the epithelia of xenograft mouse tumors, mostly enriched in blood vessels, and no apparent difference was observed between control and Artesunate-treated mice (Figure 4C). Altogether, these results suggested that the subcutaneous xenograft tumors produced less albumin than their normal liver counterpart, in consistence to the

observed human data of lower albumin in tumor as compared to normal tissue. Moreover, blood serum albumin was comparable between control and Artesunate-treated xenograft mice. Xenograft mice depicted comparable mean but less variance in blood serum albumin as compared to untreated mice.

Alternatively, although albumin was barely detectable in xenograft mouse tumor epithelia (Figure 4C), HepG2 cells expressed albumin on monolayer and organoid cultures *in vitro* (Figure 4D). Treatment with 30 μM Artesunate lowered albumin levels on monolayer and in organoids as compared to control (Figure 4D). However, even though IF staining of monolayer and organoid cultures of HepG2 cells *in vitro* depicted similar trends (Figure 4D), biochemical analysis of secreted albumin showed that monolayer cultures exhibited undetectable albumin levels, whereas organoid cultures produced albumin detected in serum-depleted culture medium, with insignificant difference between Artesunate-treated and control cells (Figure 4F). Taken together, Artesunate treatment reduced intracellular albumin in HepG2 monolayer and organoid cultures (Figure 4D), but did not alter the profile of secreted albumin by HepG2 organoids (Figure 4F). This finding demonstrated that Artesunate only affected intracellular albumin but not secreted albumin *in vitro*.

Similar to intracellular albumin reduction in both monolayer and organoid HepG2 cultures, tissue architecture did not alter Artesunate sensitivity *in vitro*. ATP release assay showed that proliferation of both HepG2 monolayer and organoid cultures treated with Artesunate slowed down as compared to corresponding controls (Figure 4G), suggesting that Artesunate was effective in both monolayer and organoid cultures. It was notable that monolayer culture induced faster proliferation than organoid culture (Figure 4G). Subsequently, the extent of proliferation retardation between Artesunate treatment and control was larger on monolayer as compared to organoid (Figure 4G), hence suggesting that the difference in the extent of proliferation retardation was a consequence of proliferation rate rather than drug efficacy. Therefore, Artesunate inhibited HepG2 proliferation *in vitro* in both monolayer and organoid cultures.

To this point, evidence pointed to the difference in intracellular albumin between *in vitro* cultures (Figure 4D) and xenograft tumor tissue (Figure 4C). Given that albumin serves as a drug carrier *in vivo* [19], we first tested if albumin binds to Artesunate to enhance intracellular uptake of Artesunate in *in vitro* cultures which depicted higher intracellular albumin. Molecular docking of Artesunate on human albumin protein predicted three binding sites (Supplementary Figure 3A). However, no binding between Artesunate and bovine serum albumin was observed up to 4.25:1 molar ratio between Artesunate and albumin using isothermal calorimetry (ITC) (Supplementary Figure 3B). To verify that our comparisons were valid, sequence alignment of human, bovine and mouse albumin proteins was performed. Results showed that the predicted binding sites were generally conserved across species (Supplementary Figure 3C), suggesting that the ITC binding experiment was relevant to imply for mouse albumin in our xenograft model. Hence, we concluded that Artesunate did not bind to albumin and that the higher intracellular albumin in *in vitro* cultures as compared to xenograft tumor could not explain the inefficacy of Artesunate *in vivo*.

In summary, *in vitro* application of Artesunate on HepG2 cells resulted in lower intracellular albumin (Figure 4D) and diminished cell viability (Figure 4G), without affecting secreted albumin (Figure 4F) in both monolayer and organoid cultures. In contrast, HepG2 xenograft tumors showed low intracellular albumin (Figure 4C) and insensitivity towards Artesunate (Figure 4A). Engrafted mice depicted high intracellular albumin in the liver (Figure 4C) and normal serum

albumin in blood (Figure 4E). Based on all prevailing evidence, albumin seemed to be consequence rather than cause of effective Artesunate treatment *in vitro*.

Lastly, we checked the blood biochemical parameters of engrafted mice under control and Artesunate treatment, in comparison to untreated mice, to investigate the impact of tumor engraftment and drug administration on physiology. Results showed that there was no significant difference in glucose, total protein and triglycerides between engrafted and untreated mice (Figure 5C). Artesunate treatment did not alter these parameters as compared to control (Figure 5C). Body weight of the different experimental groups exhibited no significant difference too (data not shown). Hence, we concluded that: (1) subcutaneous HepG2 engraftment did not alter animal physiology; and (2) Artesunate treatment did not alter animal physiology.

In conclusion, tissue architecture did not confer to Artesunate inefficacy *in vivo*, and blood biochemical parameters did not vary with tumor engraftment or Artesunate treatment.

Discussion

In this study, we showed that the Artemisinin analog Artesunate inhibited HepG2 cell proliferation and activated the Erk1/2-DAPK1 pathway to promote apoptosis *in vitro*.

Erk signaling pathway is well-known for promoting cell proliferation [20] and motility [21], both of which attributes to enhance tumorigenesis and metastasis. However, this study demonstrated the inhibition of HepG2 cell growth by Artesunate treatment *in vitro* through Erk1/2 phosphorylation. In concert to our results, strong Erk2 phosphorylation was induced by hepatocyte growth factor (HGF), leading to retarded cell proliferation in HepG2 cells, which was reversed by adding the MEK inhibitors of PD98059 or U0126 that alleviated Erk2 phosphorylation [22]. Similarly, activation of Erk1/2-DAPK1 pathway has been reported to trigger apoptosis in NIH3T3 cells under starvation [11]. Thus, stress caused by nutritional deprivation or chemotoxic insults could stimulate Erk phosphorylation to trigger apoptosis. Contrariwise, pro-proliferation studies that activated Erk1/2 involved growth factor receptor activation [20], which was absent in this study and others that demonstrated Erk-induced cell death. Hence, Erk phosphorylation itself does not determine cell fate.

In this regard, our Western blotting experiment showed different Erk phosphorylation patterns during direct drug addition and medium replacement, suggesting that experimental conditions could interfere interpretation. Nevertheless, DAPK1 dephosphorylation and lamellipodium loss was observed in Artesunate-treated cells but not in control in both scenarios, indicating that the downstream pathways were conserved. On the other hand, the MEK1 inhibitor U0126 had modest effects on caspase activation and cell proliferation in Artesunate-treated HepG2 cells before 24 h post-treatment. Thus, we hypothesized of the onset of co-stimulatory pathway(s) in addition to Erk signaling, which required further investigation.

Artesunate was ineffective in inhibiting tumor growth *in vivo*. To find out the reason, we investigated the HCC biomarkers of AFP and albumin *in vitro* and *in vivo* (Figure 5A), tissue architecture and blood biochemical parameters. Results showed that none of these attributed to drug insensitivity. Notwithstanding, intracellular albumin was reduced after Artesunate treatment *in vitro*, whereas intracellular and blood serum albumin remained stable in livers and tumors of xenograft mice regardless of treatment. Thus, we deduced that albumin reduction was a

consequence of drug administration. Using genomic sequence alignment, we identified a downstream Erk target that bound to the albumin promoter, named CCAAAT/enhancer-binding protein-beta (C/EBPβ), by TFmapper (http://www.tfmapper.org/). Overexpression of C/EBPβ was reported to downregulate albumin transcription in HepG2 cells *in vitro* [23]. Because albumin was reported to promote proliferation triggered by Erk activation in kidney cells [24, 25], reducing albumin may hinder Erk-mediated cell proliferation. Coincidently, C/EBPβ upregulated DAPK1 expression and induced apoptosis in mouse embryonic fibroblasts upon interferon-gamma (IFNγ) stimulus [26]. Therefore, C/EBPβ might provide parallel pathways to impede growth and promote death in HepG2 cells under Artesunate treatment in our current model (Figure 5B).

Given that tissue architecture did not confer to drug response and no changes on animal physiology was perceived, we wondered if the pharmacokinetics of Artesunate might attribute to drug inefficacy *in vivo*. Indeed, Morris, *et al*, demonstrated that the blood clearance rate and half-life of Artesunate was 2-3 L kg^{-1} h^{-1} and less than 15 min for intravenous injection in human patients [27]. The clearance rate and half-life was slightly higher, 19.2-30 L kg^{-1} h^{-1} and 20-45 min for oral administration, and 2.4-3.5 L kg^{-1} h^{-1} and 25-48 min for intramuscular administration, respectively [27]. Therefore, we reasoned that mice would exhibit similar clearance rate *in vivo*, thus resulting in no drug response due to rapid drug clearance. Nevertheless, given its tumor inhibition efficiency *in vitro* and mild effects *in vivo*, we hypothesized that improving drug distribution might improve Artesunate efficacy *in vivo*.

Materials and Methods

Drugs and Reagents

Artesunate (CAS# 88495-63-0) and Dihydroartemisinin (CAS# 71939-50-9) were bought from Shanghai Aladdin Bio-Chem Technology Company Limited, China. Artemisinin (CAS# 63968-64-9) and Artemether (CAS# 71963-77-4) were bought from Carbosynth Limited, UK. Cell culture medium and auxiliary components were bought from Life Technologies, USA. Matrigel® (Cat# 356235) was bought from Corning, USA. All other reagents were bought from Sigma-Aldrich, USA, unless otherwise indicated. Antibodies used in this study were listed in Supplementary Table 1.

Cell culture

The indicated cell lines were obtained from Professor Chuxia Deng's laboratory.

All cells were cultured on monolayer with Dulbecco's Modified Eagle Medium (DMEM) or RPMI 1640 medium supplemented with 10% fetal bovine serum (FBS), 100 U/mL Penicillin-Stretomycin and 2 mM L-glutamine. Cells were incubated at 37°C in a 5% CO_2 humidified incubator and passaged every 3-4 d.

For HepG2 organoid culture, HepG2 cells passaged on monolayer were resuspended as 30,000 cells/mL final concentration in 1:1 (v/v) Matrigel® : 3D medium comprising of Advanced DMEM/F12 medium supplemented with 100 U/mL Penicillin-Stretomycin, 1% (v/v) GlutaMAX™, 10 mM HEPES pH7.4, 1x B-27™ Supplement without Vitamin A, 1x N-2 supplement, 1.25 mM N-acetyl-L-cysteine, 10 mM Nicotinamide, 10 nM recombinant human [Leu^{15}]-Gastrin I, 50 ng/mL recombinant human Epidermal Growth Factor (EGF), 10 μM Forskolin, 5 μM A8301

(Selleckchem, USA) and 10 μM Y27632 (Selleckchem, USA). Resuspended cells were seeded in 30uL droplets at the bottom of 6-well plate and 2 mL 3D medium was applied. Cells were incubated at 37°C in a 5% CO_2 humidified incubator and passaged every 4 d.

For immunofluorescence staining, organoids were cultured in 3D medium supplemented with 1% (w/v) of 1:2 (w/w) gelatin : agar on 4-well chamber slides, and subject to fixation.

Drug screening and IncuCyte® analysis

Cells were seeded at 2,000-8,000 cells/well in 30 μL cell culture medium on a 384-well clear-bottom square-well plate. 3 μL of serially diluted 10x concentration of each drug, yielding a dose gradient from 200 μM to 12.8 nM final concentration, was added to each well in quadruplicates immediately after cell seeding. The cells were incubated at 37°C in a 5% CO_2 humidified incubator for 72 h. Relative cell viability was measured by fluorescence at ex. 560 nm / em. 590 nm using Alamar Blue assay [28] on Molecular Devices SpectraMax M5 Plate Reader. 0.1% dimethyl sulfoxide (DMSO) was used as negative control and cell-free medium was setup as blank control.

For IncuCyte® analysis, HepG2 cells were seeded at 5,000 cells/well in 100 μL cell culture medium on a 96-well plate. The cells were incubated at 37°C in a 5% CO_2 humidified incubator overnight before a final concentration of 30 μM Arteusnate and/or 5 μM U0126 was applied. Immediately after drug addition, the cells were transferred to Satorius IncuCyte® Live Cell Imaging System. Each treatment condition contained triplicate wells, where 4 field of views (FOVs) per well were imaged at 2 h intervals for 74 h in total. 0.1% DMSO was used as negative control.

Intracellular iron measurement

Sampled tissue from different mouse organs were freshly cut immediately after mouse euthanization, followed by three washes with phosphate buffered saline (PBS). Sampled cells were grown to confluence in a 6-well plate under normal culture conditions, trypsinized, counted and washed with PBS thrice. Afterwards, the samples were freeze-dried into dry powder and weighed. 1 mL concentrated nitric acid was applied to dissolve all samples by microwave. The extract was diluted and metered to 50 mL with pure water. 5 mL of the diluted extract was sent for ionization coupled plasma atomic emission spectroscopy (ICP-AES) analysis at the Analytic Centre of Jinan University, Guangzhou, China. The measured iron concentrations were finally converted to mg/g tissue (dry weight) or pg/cell based on arithmetic calculation.

Cell cycle analysis

HepG2 cells were initially treated with 0.1% DMSO or 10-50 μM Artemisinin and its derivatives on a 6-well plate at 37°C in a 5% CO_2 humidified incubator for 12 h. Cells were trypsinized and transferred to 4 mL round-bottom tubes. 2 volumes of pure ethanol were added in a dropwise manner on slow vortex. After the cells were fixed, final concentration of 5 μg/mL propidium iodide (PI) (Life Technologies, USA) and 1 mg/mL RNase I (Life Technologies, USA) was added to stain the cells for 10 min. Lastly, the cells were filtered through 40 μm cell strainer and loaded on BD FACS Calibur Flow Cytometer for cell cycle analysis by flow cytometry.

Radical oxygen species (ROS) staining

HepG2 cells were treated with doses of 10-50 μM Artemisinin and its derivatives on a 6-well plate at 37°C in a 5% CO_2 humidified incubator for 12 h. After drug treatment, cells were first washed with PBS thrice. Then a final concentration of 10 μM Carboxyl-H_2DCFDA (Life Technologies, USA) was added to each well and incubated at room temperature for 10-20 min. Cells were immediately imaged under green fluorescence channel at 10x magnification using Life Technologies EVOS FL Imaging System. Carbonylcyanide-4-(trifluoromethoxy)-phenylhydrazone (FCCP) (Enzo Life Sciences, Hong Kong) was used as positive control, 0.1% DMSO was used as negative control.

Intracellular pH measurement

HepG2 cells were initially treated with 0.1% DMSO or 30 μM of Artesunate on a 24-well plate at 37°C in a 5% CO_2 humidified incubator for 12 h. Then a final concentration of 0.5 μM 2',7'-bis-(2-carboxyethyl)-5-(and-6)-carboxyfluorescein (BCECF) (Life Technologies, USA) was added to each well and incubated at room temperature for 30 min, followed by plate reading at ex. 440 nm / em. 535 nm and ex. 490 nm / em. 535 nm using Molecular Devices SpectraMax M5 Plate Reader. A standard curve was plotted using home-made buffers constituting a pH gradient from 6.5 to 8.5.

Western blotting

HepG2 cells were initially treated with 0.1% DMSO or 30 μM of Artesunate, in the absence and presence of 5 μM U0126, on a 6-well plate at 37°C in a 5% CO_2 humidified incubator for the indicated time on each figure. Cells were then washed with PBS thrice. Subsequently, gel loading dye was directly applied to the adherent cells, incubated at room temperature for 10 min, and transferred to heat-block for protein denaturation at 95°C for 10 min. Protein samples were separated on 10% or 15% SDS-PAGE followed by Western blotting using specific antibodies. Blots were scanned by near-infrared fluorescence using Licor Odyssey CLx Imager.

Immunofluorescence

HepG2 cells in monolayer or organoid culture were initially treated with 0.1% DMSO or 30 μM of Artesunate, in the absence and presence of 5 μM U0126, on a 4-well chamber slide at 37°C in a 5% CO_2 humidified incubator for 12 h. Cells were then washed with PBS thrice. Subsequently, cells were fixed with 10% Formalin and washed with 1% Triton X-100, followed by specific antibody staining. 10x to 40x magnified images were taken using Olympus BX83 Upright Fluorescent Microscope, whereas 63x magnified images were taken on Carl Zeiss LSM 710 Confocal Fluorescent Microscope.

Xenograft mouse model

All mouse experiments were approved by the Animal Research Ethics Committee of University of Macau under protocol UMARE-050-2017. 3.0×10^6 HepG2 cells suspended in 1:1 (v/v) Matrigel® : PBS was implanted subcutaneously on the left and right flank of athymic nude mice (Balb/c Nude). Tumorigenesis occurred between 10-14 d. When tumors reached 2 mm in any dimension, the mice were separated into two groups of 10 mice. Each group of mice was subject to intraperitoneal injection of 50 mg/kg Artesunate in 0.4% Tween-80 in PBS and solvent

alone, respectively, at a frequency of 2 times per week for a total span of 4 weeks or until the tumor exceeded 1.5 cm^3 in any dimension.

Before euthanasia, mice underwent anesthesia by 250 mg/kg Avertin. Blood was extracted from the heart with ethylenediaminetetraacetic acid (EDTA) as anti-coagulant. Tumors and other relevant organs were resected after euthanasia.

Hematoxylin and eosin (H&E) staining and immunohistochemistry (IHC)

Resected tumors and organs were immersed in Thermo Fisher Cryochrome™ embedding resin, and stored at -80°C until use. The frozen blocks were cut into 5-10 μm slices using Leica CM3050S Cryostat. The slices were transferred to 25 × 75 mm positive adhesion glass slides and fixed in 10% Formalin, followed by H&E staining following standard procedures or antibody staining following manufacturer's instructions for Thermo Fisher Histostain-*Plus* IHC Kit. IHC slides were counterstained by Hematoxylin. All slides were dehydrated by xylene and mounted by DPX Mountant. 10x magnified images were taken using Olympus BX83 Upright Fluorescent Microscope.

Blood biochemistry

Immediately after extraction, whole blood was centrifuged at 10,000g at room temperature for 2 min. Plasma was aspirated and transferred to a new microfuge tube. Plasma was stored at -80°C if necessary. Plasma was loaded on Sysmex BX-3000 Automated Chemistry Analyzer calibrated using Biosystems Biochemistry Multi-calibrator and Biosystems Lipid Control Serum II, respectively. Results were automatically calculated by the complimentary software.

Isothermal calorimetry

Isothermal calorimetry (ITC) was performed in the Drug Development Core, Faculty of Health Sciences, University of Macau. 200 μM Artesunate was titrated into 5μM bovine serum albumin (BSA) at 25°C on GE Healthcare Microcal iTC200 system. The solvent was phosphate buffered saline (PBS); BSA solvent was supplemented with 0.1% DMSO to match the ligand solvent.

Acknowledgement

Acknowledgements to Mr. Zepeng Jiao of Analytic Centre, Jinan University for instructions on ICP-AES, Dr. Peng Lyu of Prof. Henry Kwok's lab for instructions on IncuCyte®, Dr. Qiang Chen of Prof. Chuxia Deng's lab and Dr. Weiwei Liu of Bioimaging Core for supervision on FACS, Dr. Xiaohui Hu of Drug Development Core for supervision and assistance with ITC, Mr. Joshua Cai, Ms. Avery Tam and Mr. Kevin Tang of Animal Facility for supervision and assistance on mouse experiments, Dr. Jammy Chan of Kiang Wu Hospital for advice on histology, Prof. Wenhua Zheng for provision of Artemisinin and analogs, Prof. Qian Luo for provision of Sensor C3 reporter plasmid, and Prof. Joong Sup Shim for provision of BCECF.

Conflict of Interest

The authors declared no conflict of interest.

Author Contributions

S.L.S., A.H.W. and C.D. conceived this project. J.K.W., S.L.S. and K.H.W. were supervised by A.H.W. A.H.W. designed experiments and analyzed results. J.K.W., S.L.S., K.H.W. and A.H.W. performed experiments; H.W. wrote R scripts for data analysis; F.X. constructed the Sensor C3-labelled HepG2 cell line; Y.Q. provided 3D medium and instructions on organoid culture. All authors prepared the manuscript. This project was supported by Macao Science and Technology Development Fund (FDCT) FDCT/137/2016/A granted to A.H.W. and FDCT/094/2015/A3 granted to C.D. All authors read and approved of publication of this manuscript.

References

1. NBSC. *China Statistics Yearbook 2017*. 2017; Available from: http://www.stats.gov.cn/tjsj/ndsj/2017/indexeh.htm.
2. NCCN. *NCCN Guidelines for Treatment of Cancer by Site*. 2018; Available from: https://www.nccn.org/.
3. Tu, Y., *The discovery of artemisinin (qinghaosu) and gifts from Chinese medicine.* Nat Med, 2011. **17**(10): p. 1217-20.
4. Zeng, Z., J. Xu, and W. Zheng, *Artemisinin protects PC12 cells against beta-amyloid-induced apoptosis through activation of the ERK1/2 signaling pathway.* Redox Biol, 2017. **12**: p. 625-633.
5. Efferth, T., et al., *The antiviral activities of artemisinin and artesunate.* Clin Infect Dis, 2008. **47**(6): p. 804-11.
6. Konstat-Korzenny, E., et al., *Artemisinin and Its Synthetic Derivatives as a Possible Therapy for Cancer.* Med Sci (Basel), 2018. **6**(1).
7. Sundar, S.N., et al., *Artemisinin selectively decreases functional levels of estrogen receptor-alpha and ablates estrogen-induced proliferation in human breast cancer cells.* Carcinogenesis, 2008. **29**(12): p. 2252-8.
8. Mercer, A.E., et al., *Evidence for the involvement of carbon-centered radicals in the induction of apoptotic cell death by artemisinin compounds.* J Biol Chem, 2007. **282**(13): p. 9372-82.
9. Li, Y., et al., *Novel antitumor artemisinin derivatives targeting G1 phase of the cell cycle.* Bioorg Med Chem Lett, 2001. **11**(1): p. 5-8.
10. Blazquez, A.G., et al., *Novel artemisinin derivatives with potential usefulness against liver/colon cancer and viral hepatitis.* Bioorg Med Chem, 2013. **21**(14): p. 4432-41.
11. Chen, C.H., et al., *Bidirectional signals transduced by DAPK-ERK interaction promote the apoptotic effect of DAPK.* EMBO J, 2005. **24**(2): p. 294-304.
12. Singh, P., P. Ravanan, and P. Talwar, *Death Associated Protein Kinase 1 (DAPK1): A Regulator of Apoptosis and Autophagy.* Frontiers in Molecular Neuroscience, 2016. **9**: p. 46.
13. Shani, G., et al., *Autophosphorylation restrains the apoptotic activity of DRP-1 kinase by controlling dimerization and calmodulin binding.* EMBO J, 2001. **20**(5): p. 1099-113.
14. Shohat, G., et al., *The pro-apoptotic function of death-associated protein kinase is controlled by a unique inhibitory autophosphorylation-based mechanism.* J Biol Chem, 2001. **276**(50): p. 47460-7.
15. Roskoski, R., Jr., *ERK1/2 MAP kinases: structure, function, and regulation.* Pharmacol Res, 2012. **66**(2): p. 105-43.

16. Luo, K.Q., et al., *Application of the fluorescence resonance energy transfer method for studying the dynamics of caspase-3 activation during UV-induced apoptosis in living HeLa cells.* Biochem Biophys Res Commun, 2001. **283**(5): p. 1054-60.
17. Wong, A.H., et al., *Drug screening of cancer cell lines and human primary tumors using droplet microfluidics.* Sci Rep, 2017. **7**(1): p. 9109.
18. Fu, J. and H. Wang, *Precision diagnosis and treatment of liver cancer in China.* Cancer Lett, 2018. **412**: p. 283-288.
19. Raoufinia, R., et al., *Overview of Albumin and Its Purification Methods.* Adv Pharm Bull, 2016. **6**(4): p. 495-507.
20. Caunt, C.J., et al., *MEK1 and MEK2 inhibitors and cancer therapy: the long and winding road.* Nat Rev Cancer, 2015. **15**(10): p. 577-92.
21. Tanimura, S. and K. Takeda, *ERK signalling as a regulator of cell motility.* J Biochem, 2017. **162**(3): p. 145-154.
22. Tsukada, Y., K. Miyazawa, and N. Kitamura, *High intensity ERK signal mediates hepatocyte growth factor-induced proliferation inhibition of the human hepatocellular carcinoma cell line HepG2.* Journal of Biological Chemistry, 2001. **276**(44): p. 40968-40976.
23. Trautwein, C., et al., *C/EBP-beta/LAP controls down-regulation of albumin gene transcription during liver regeneration.* (0021-9258 (Print)).
24. Cohen, M.P., E. Shea, and C.W. Shearman, *ERK mediates effects of glycated albumin in mesangial cells.* Biochemical and Biophysical Research Communications, 2001. **283**(3): p. 641-643.
25. Reich, H., et al., *Albumin activates ERK Via EGF receptor in human renal epithelial cells.* Journal of the American Society of Nephrology, 2005. **16**(5): p. 1266-1278.
26. Gade, P., et al., *Critical Role for Transcription Factor C/EBP-β in Regulating the Expression of Death-Associated Protein Kinase 1.* Molecular and Cellular Biology, 2008. **28**(8): p. 2528.
27. Morris, C.A., et al., *Review of the clinical pharmacokinetics of artesunate and its active metabolite dihydroartemisinin following intravenous, intramuscular, oral or rectal administration.* Malaria journal, 2011. **10**: p. 263-263.
28. O'Brien, J., et al., *Investigation of the Alamar Blue (resazurin) fluorescent dye for the assessment of mammalian cell cytotoxicity.* Eur J Biochem, 2000. **267**(17): p. 5421-6.

Artesunate pErk up HepG2 cells to die through apoptosis *in vitro*

Johnny Kuan-Un Wong *[,1], Sophie Ling Shi *[,1], Haitao Wang [1], Fuqiang Xing [1], Yingyao Quan [1], Kristy Hio-Meng Wong [2], Ada Hang-Heng Wong #[,1], Chuxia Deng #[,1]

[1] Cancer Centre, Faculty of Health Sciences, University of Macau, Macau S.A.R., China.

[2] Summer Program for Secondary School Students, Faculty of Health Sciences, University of Macau, Macau S.A.R., China.

Correspondence: adahhwong@um.edu.mo (A.H.W.), cxdeng@um.edu.mo (C.D.)

Figure Legends

Figure 1. Artesunate did not inhibit HepG2 cell proliferation by known Artemisinin modes of action. (A) Drug screening and intracellular iron measurement of cancer cell lines. A sum of eleven cancer cell lines from six tissue origins were screened against four analogs of Artemisinin. Cell viability was assessed by Alamar Blue assay and intracellular iron was measured by ionization coupled plasma atomic emission spectroscopy. Quadriplicates were used for drug screening and single point measurement was used for intracellular iron measurement. (B) Drug response curves of HepG2 treated with four Artemisinin analogs. HepG2 cells were treated with gradient doses of Artemisinin and its derivatives from 200 μM to 12.8 nM for 3 d, and subject to Alamar Blue assay. The mean and standard deviation of normalized cell viability from quadruplicate experiments was plotted against the log of drug concentration. (C) Fluorescence activated cell sorting of Artesunate-treated HepG2 cells. 30 μM Artesunate was applied to HepG2 cells and treated for 12 h, and subject to fluorescence activated cell sorting after propidium iodide staining. (D) Iron measurement of mouse organs. Organs were dissected from one untreated athymic nude mouse after euthanasia, and subject to by ionization coupled plasma atomic emission spectroscopy for iron measurement. Iron concentration per gram (mg/g) of tissue was plotted against the investigated tissue. (E) Correlation between IC_{50} values after Artesunate treatment and intracellular iron concentration of all investigated cell lines. IC_{50} values of the eleven investigated cell lines after Artesunate treatment were plotted against corresponding intracellular iron concentration of respective cell lines. Each dot represented one cell line and the color of the dot denoted the tissue origin of the indicated cell line. (F) Radical oxygen species staining of Artesunate-treated HepG2 cells. HepG2 cells were treated with IC_{50} concentrations of the four Artemisinin analogs for 12 h, and subject to carboxy-H_2DCFDA staining followed by fluorescence imaging under 10x objective for radical oxygen species detection. FCCP and DMSO were used as positive and negative controls respectively. (G) pH measurement of Artesunate-treated HepG2 cells. HepG2 cells were treated with IC_{50} concentrations of the four Artemisinin analogs for 12 h, and subject to BCECF staining followed by fluorescence plate reading for pH measurement. Each dot represented one data point, whereas the mean and standard deviation was represented by the column and error bar. Standard curve measurements from standard pH buffers was used for pH calibration.

Figure 2. Artesunate inhibited HepG2 cell proliferation via Erk1/2-DAPK1 pathway *in vitro*. (A) Western blotting of Artesunate-treated HepG2 cells against different kinase antibodies. 30 μM Artesunate was applied to HepG2 cells and treated over a time course of 24 h. Parallel blotting of phosphorylated and total proteins was performed. (B) Gene structure of DAPK1 kinase. DAPK1

is a multi-domain kinase that participates in apoptosis and autophagy. (C) Western blotting of Erk1/2-DAPK1 pathway proteins during Artesunate treatment. Western blotting was performed on HepG2 cells treated with 30 μM Artesunate and/or 5 μM U0126 over a time course of 24 h. Parallel blotting of phosphorylated proteins was performed; α-tubulin and GAPDH was used as loading controls. (D) Western blotting of cell death-related proteins in Artesunate-treated HepG2 cells. 30 μM Artesunate was applied to HepG2 cells and treated over a time course of 24 h. (E) Caspase activation assay on Artesunate-treated HepG2 cells. Caspase-Glo® assay was performed on HepG2 cells treated with 30 μM Artesunate and/or 5 μM U0126 over a time course of 48 h. The mean and standard deviation from quadruplicate experiments of relative caspase activity were plotted against time (h). (F) Cell death assay on Artesunate-treated HepG2 cells. IncuCyte® time-lapse imaging was performed on HepG2 cells treated with 30 μM Artesunate and/or 5 μM U0126 over a time course of 30 h. The mean and standard deviation of arbitrary confluence from 4 field of views in triplicate experiments were plotted against time (h).

Figure 3. Multiploidy formation induced by U0126 abrogated its rescue effect on Artesunate-treated HepG2 cells. (A) Cell proliferation assay of HepG2 cells under Artesunate treatment alone or in combination with U0126. Alamar Blue assay was performed on HepG2 cells treated with 30 μM Artesunate and/or 5 μM U0126 over a time course of 72 h. (B) Cell proliferation assay of HepG2 cells under Artesunate treatment alone or in combination with U0126. IncuCyte® time-lapse imaging was performed on HepG2 cells treated with 30 μM Artesunate and/or 5 μM U0126 over a time course of 74 h. (C) Cell morphology analysis of IncuCyte® time-lapse images. Images of the IncuCyte® time-lapse imaging experiment was analyzed to observe changes in cell morphology in HepG2 cells treated with 30 μM Artesunate and/or 5 μM U0126 over a time course of 74 h. (D) Immunofluorescence staining of cytoskeleton of HepG2 cells under Artesunate treatment alone or in combination with U0126. HepG2 cells treated with 30 μM Artesunate and/or 5 μM U0126 for 12 h were fixed and stained against DAPI (nucleus), α-tubulin antibody and phalloidin (β-actin), followed by fluorescence imaging under 20x objective. (E) Multiploidy analysis of HepG2 cells under Artesunate treatment alone or in combination with U0126. Analysis of the immunofluorescence staining result of HepG2 cells treated with 30 μM Artesunate and/or 5 μM U0126 for 12 h was conducted to count the number of diploid and triploid cells among centrosome-distinguishable mitotic cells. (F) Cell cycle analysis of HepG2 cells under Artesunate treatment alone or in combination with U0126. Propidium iodide staining of fixed HepG2 cells treated with 30 μM Artesunate and/or 5 μM U0126 over a time course of 24 h was analyzed by fluorescence activated cell sorting.

Figure 4. Artesunate was ineffective *in vivo*. (A) Subcutaneous xenograft mouse model of HepG2 cells. HepG2 cells was subcutaneously implanted in athymic nude mice and administered with 50 mg/kg Artesunate two times per week by intraperitoneal injection for 30 d; parallel treatment with solvent alone was performed in control mice. Tumor size was measured at indicated time intervals. Tumors were finally fixed and stained by hematoxylin and eosin after euthanasia, followed by brightfield imaging under 4x objective. (B) Immunohistochemical staining of AFP in treated xenograft and untreated normal mice. Tumors and livers of control and Artesunate-treated xenograft mice were fixed and stained with AFP antibody; parallel staining of untreated normal nude mice was performed. Brightfield images were taken using 4x objective. (C) Immunohistochemical staining of albumin in treated xenograft and untreated normal mice. Tumors and livers of control and Artesunate-treated xenograft mice were fixed and stained with albumin antibody; parallel staining of untreated normal nude mice was performed. Brightfield images were

taken using 4x objective. (D) Immunofluorescence staining of AFP and albumin in HepG2 monolayer and organoid cultures after Artesunate treatment. HepG2 cells on monolayer or in organoid cultures were fixed and stained with AFP and albumin, respectively, under control or Artesunate treatment. Fluorescence images were taken under 20x objective for monolayer cultures and 60x objective for organoid cultures. (E) Blood biochemistry of HepG2 xenograft mice. Blood serum was extracted from control and Artesunate-treated xenograft mice, and subject to biochemical analysis for albumin concentration; blood sera from untreated normal mice was measured in parallel. (F) Secreted albumin measurement in HepG2 monolayer and organoid cultures after Artesunate treatment. Serum-depleted culture medium was incubated with HepG2 cells on monolayer and in organoid cultures under control and Artesunate treatment for 12 h, and subject to biochemical analysis for albumin concentration (g/L). Albumin concentration detected from serum-depleted culture medium was used as blank. (G) Cell proliferation assay of HepG2 monolayer and organoid cultures after Artesunate treatment. 30 μM Artesunate was applied to HepG2 cells on monolayer or in organoid cultures for 2 d, and subject to ATP release assay following manufacturer's protocol.

Figure 5. Artesunate inhibited HepG2 cell cultures via Erk1/2-DAPK1 pathway *in vitro*, but was ineffective *in vivo* with no explicit impact on HCC biomarkers and blood biochemistry. (A) Comparison between *in vitro* and *in vivo* models. Artesunate reduced intracellular albumin in HepG2 monolayer and organoid cultures *in vitro*, but did not alter HCC biomarkers or blood biochemical parameters *in vivo*. (B) Working hypothesis of Artesunate effects *in vitro*. Artesunate triggered lamellipodia loss and apoptosis via Erk1/2-DAPK1 pathway in HepG2 cells *in vitro*, which was not reversed by U0126 due to its independent effects. Greyed out portions of the hypothesis were not supported by empirical evidence in this study. (C) Blood biochemical analysis of treated xenograft and untreated normal mice. Blood serum was extracted from control or Artesunate-treated HepG2 xenograft mice, and untreated normal mice, and subject to biochemical analysis for absolute concentrations of glucose (mg/dL), total protein (g/L) and triglycerides (mg/dL). The mean and standard deviation of measured values of each group was represented by the column and error bar.

A

Cancer cell lines	Cancer type	Iron (pg/cell)	IC50 (μM)			
			Artemisinin	Artesunate	Dihydroartemisinin	Artemether
QBC939	Liver (Cholangiocarcinoma)	205.40	N.R.	6.03	11.48	N.R.
HCCC9810		179.28	N.R.	18.62	12.02	N.R.
BEL-7402	Liver (Hepatocellular carcinoma)	161.05	N.R.	12.02	107.15	N.R.
SMC-7721		84.64	N.R.	15.49	77.62	N.R.
Huh7		69.21	N.R.	91.20	N.R.	N.R.
HepG2		55.56	1.17	28.84	53.70	12.59
A549	Lung	117.37	N.R.	11.75	44.67	177.83
Panc1	Pancreas	112.00	N.R.	12.30	38.02	165.96
MDA-MB-231	Breast	57.05	N.R.	54.95	162.18	N.R.
Hela	Cervical	36.43	134.90	20.42	53.70	223.87
Hct116	Colon	19.28	N.R.	17.78	85.11	N.R.

N.R. denotes No Response.

B

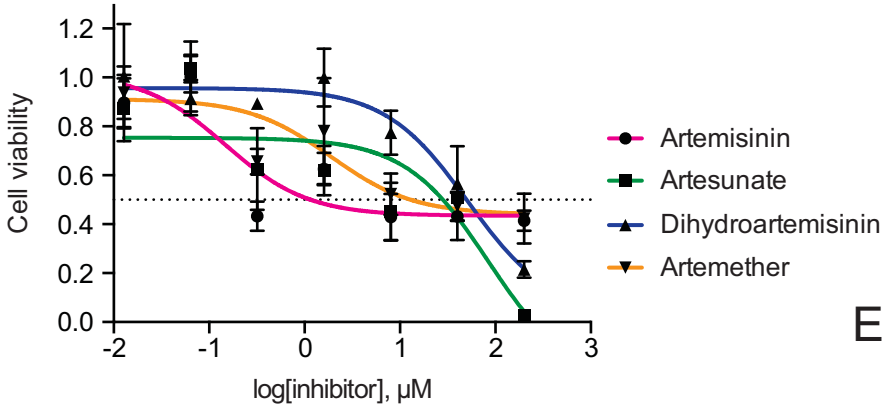

C

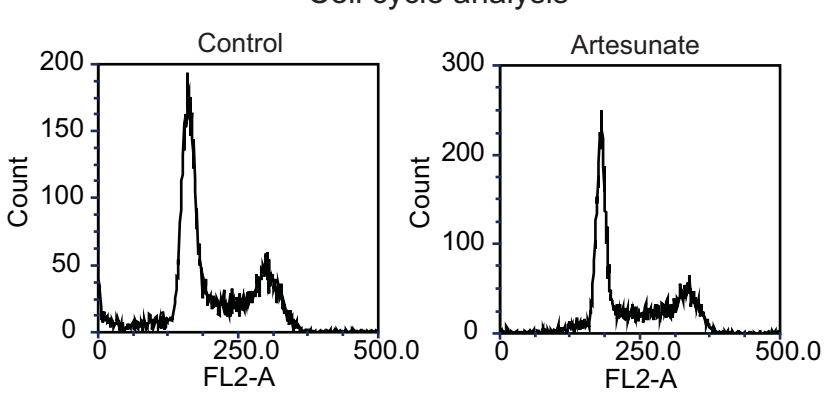

D

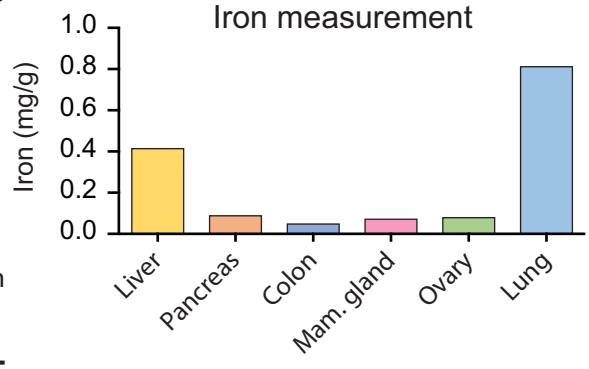

E

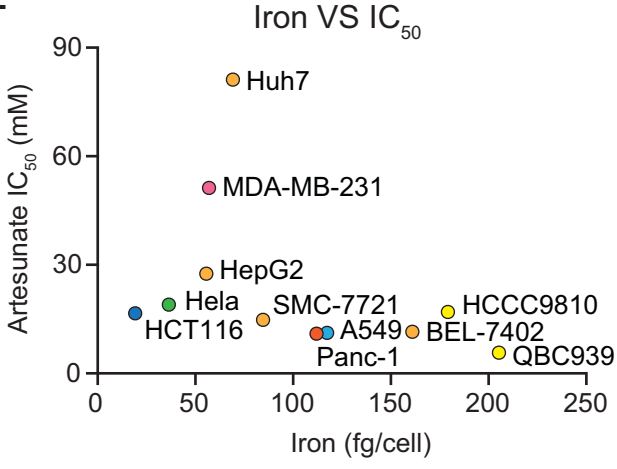

F

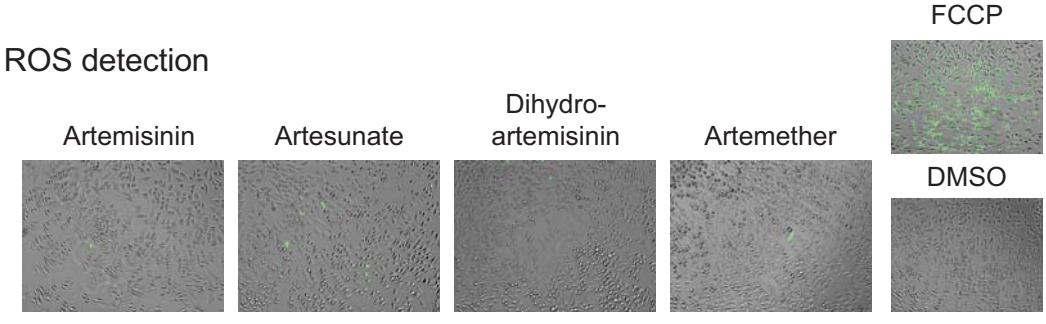

Fluorescence: Carboxy-H_2DCFDA

G

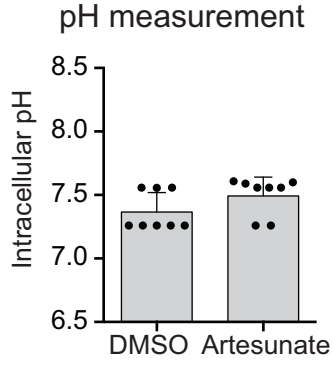

Intracellular pH: BCECF

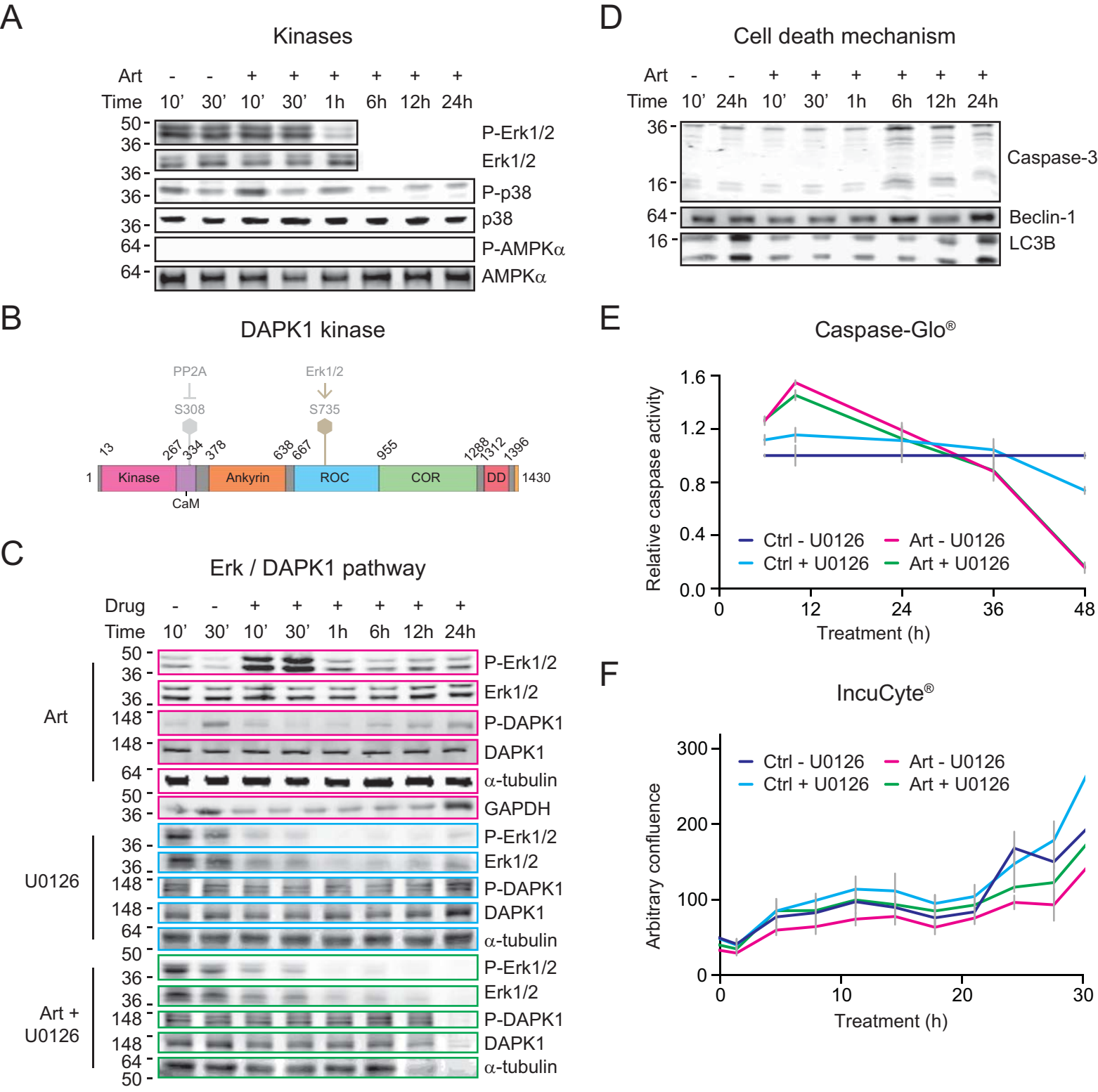
A
Kinases
Art - - + + + + + +
Time 10' 30' 10' 30' 1h 6h 12h 24h
50
36
P-Erk1/2
Erk1/2
36
P-p38
36
p38
64
P-AMPKα
64
AMPKα
B
DAPK1 kinase
PP2A
S308
Erk1/2
S735
13
267
334
378
638
667
955
1288
1312
1396
1
Kinase
Ankyrin
ROC
COR
DD
1430
CaM
C
Erk / DAPK1 pathway
Drug - - + + + + + +
Time 10' 30' 10' 30' 1h 6h 12h 24h
Art
U0126
Art + U0126
P-Erk1/2
Erk1/2
P-DAPK1
DAPK1
α-tubulin
GAPDH
D
Cell death mechanism
Art - - + + + + + +
Time 10' 24h 10' 30' 1h 6h 12h 24h
36
16
Caspase-3
64
Beclin-1
16
LC3B
E
Caspase-Glo®
Relative caspase activity
1.6
1.2
0.8
0.4
0.0
Ctrl - U0126
Art - U0126
Ctrl + U0126
Art + U0126
0
12
24
36
48
Treatment (h)
F
IncuCyte®
Arbitrary confluence
300
200
100
0
Ctrl - U0126
Art - U0126
Ctrl + U0126
Art + U0126
0
10
20
30
Treatment (h)

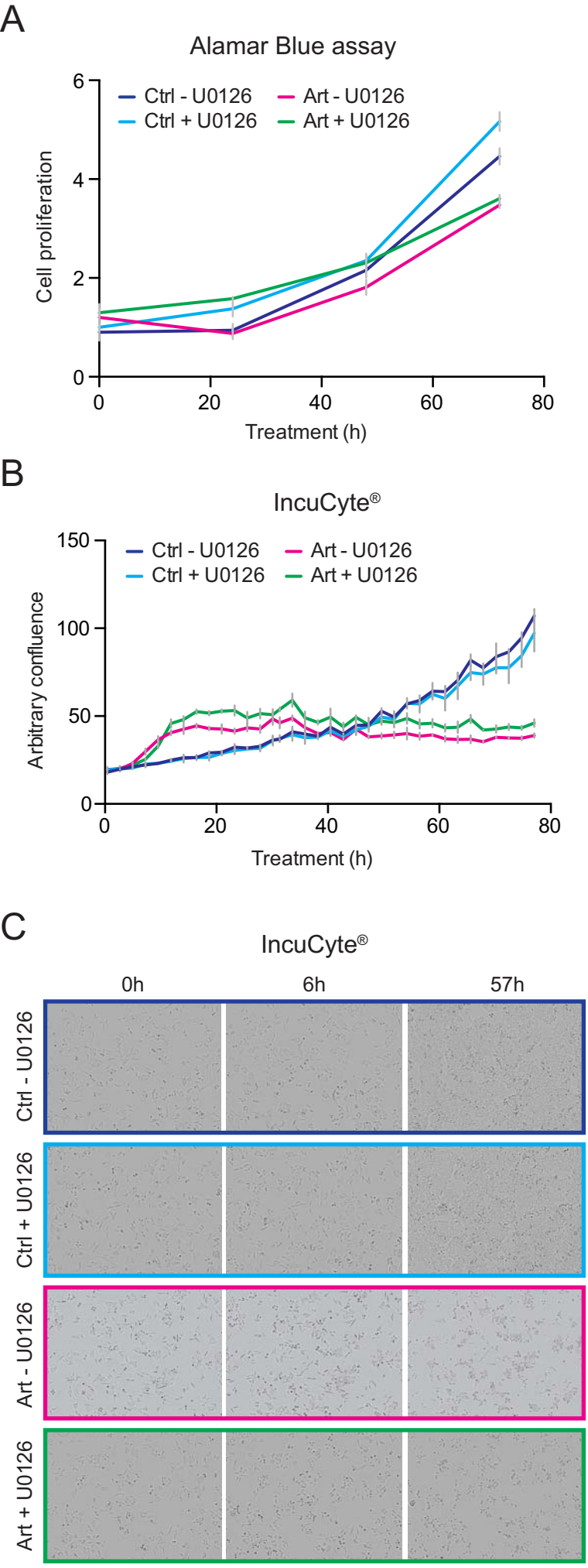
A
Alamar Blue assay
Ctrl - U0126
Ctrl + U0126
Art - U0126
Art + U0126
Cell proliferation
Treatment (h)
B
IncuCyte®
Arbitrary confluence
C
IncuCyte®
0h
6h
57h
Ctrl - U0126
Ctrl + U0126
Art - U0126
Art + U0126
D
Cytoskeleton
U0126
Ctrl
Art
Fluorescence: DAPI α-tubulin phalloidin
E
Multiploidy
% Triploid cells
3.8%
8.6%
16.8%
20.4%
% mitotic cells
Diploid
Triploid
Treatment conditions
Ctrl
Art
Art + U0126
U0126
Fluorescence: DAPI α-tubulin phalloidin
F
Cell Cycle
G1/S
G2/M
% singlet cells
Treatment (h)
FACS: Propidium iodide staining

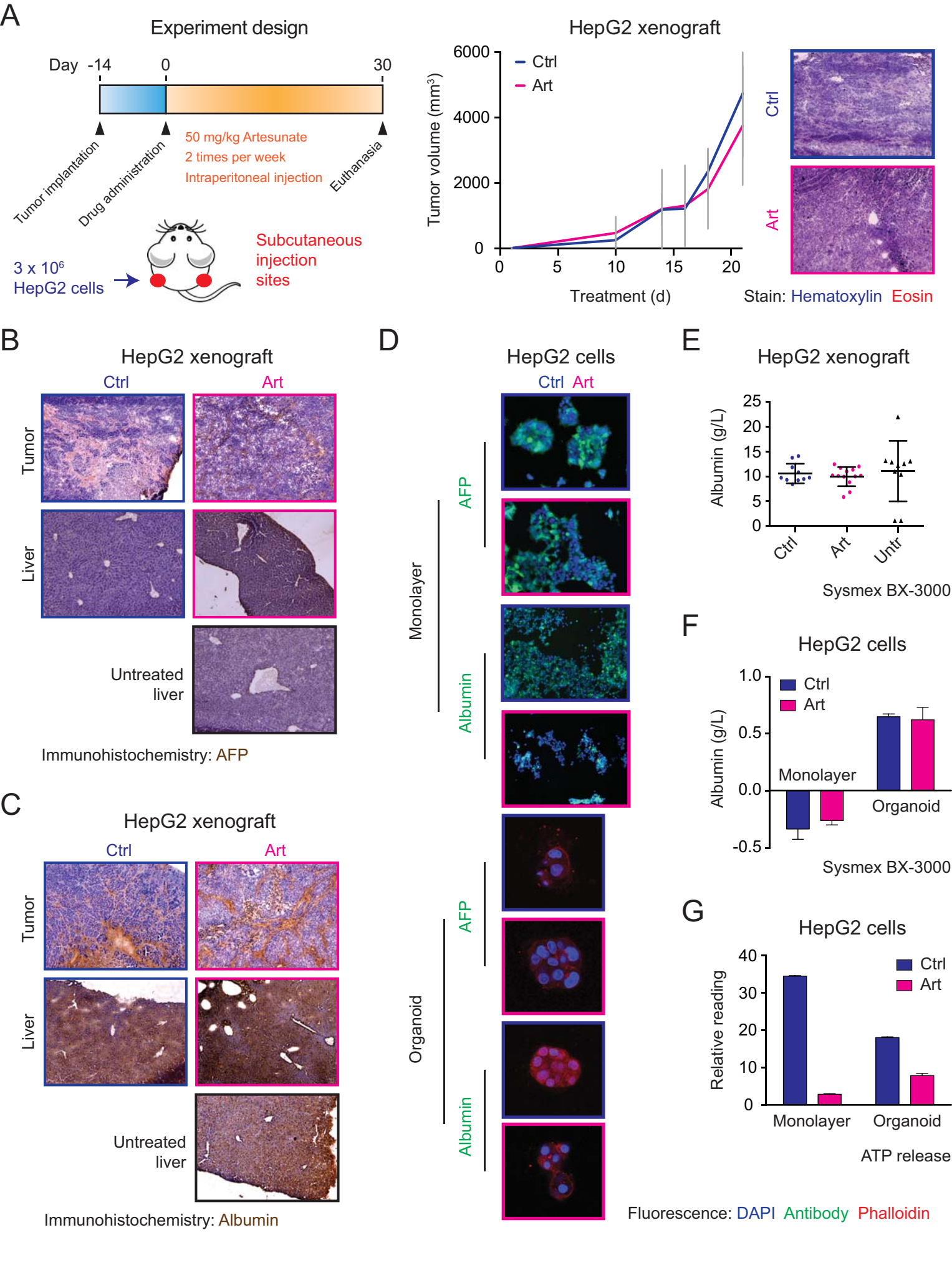
A
Experiment design
Day -14
0
30
Tumor implantation
Drug administration
Euthanasia
50 mg/kg Artesunate
2 times per week
Intraperitoneal injection
3 x 10^6
HepG2 cells
Subcutaneous
injection
sites
HepG2 xenograft
Ctrl
Art
Tumor volume (mm^3)
6000
4000
2000
0
0
5
10
15
20
Treatment (d)
Ctrl
Art
Stain: Hematoxylin Eosin
B
HepG2 xenograft
Ctrl
Art
Tumor
Liver
Untreated
liver
Immunohistochemistry: AFP
C
HepG2 xenograft
Ctrl
Art
Tumor
Liver
Untreated
liver
Immunohistochemistry: Albumin
D
HepG2 cells
Ctrl Art
Monolayer
AFP
Albumin
Organoid
AFP
Albumin
Fluorescence: DAPI Antibody Phalloidin
E
HepG2 xenograft
Albumin (g/L)
25
20
15
10
5
0
Ctrl
Art
Untr
Sysmex BX-3000
F
HepG2 cells
Albumin (g/L)
1.0
0.5
0.0
-0.5
Ctrl
Art
Monolayer
Organoid
Sysmex BX-3000
G
HepG2 cells
Relative reading
40
30
20
10
0
Ctrl
Art
Monolayer
Organoid
ATP release

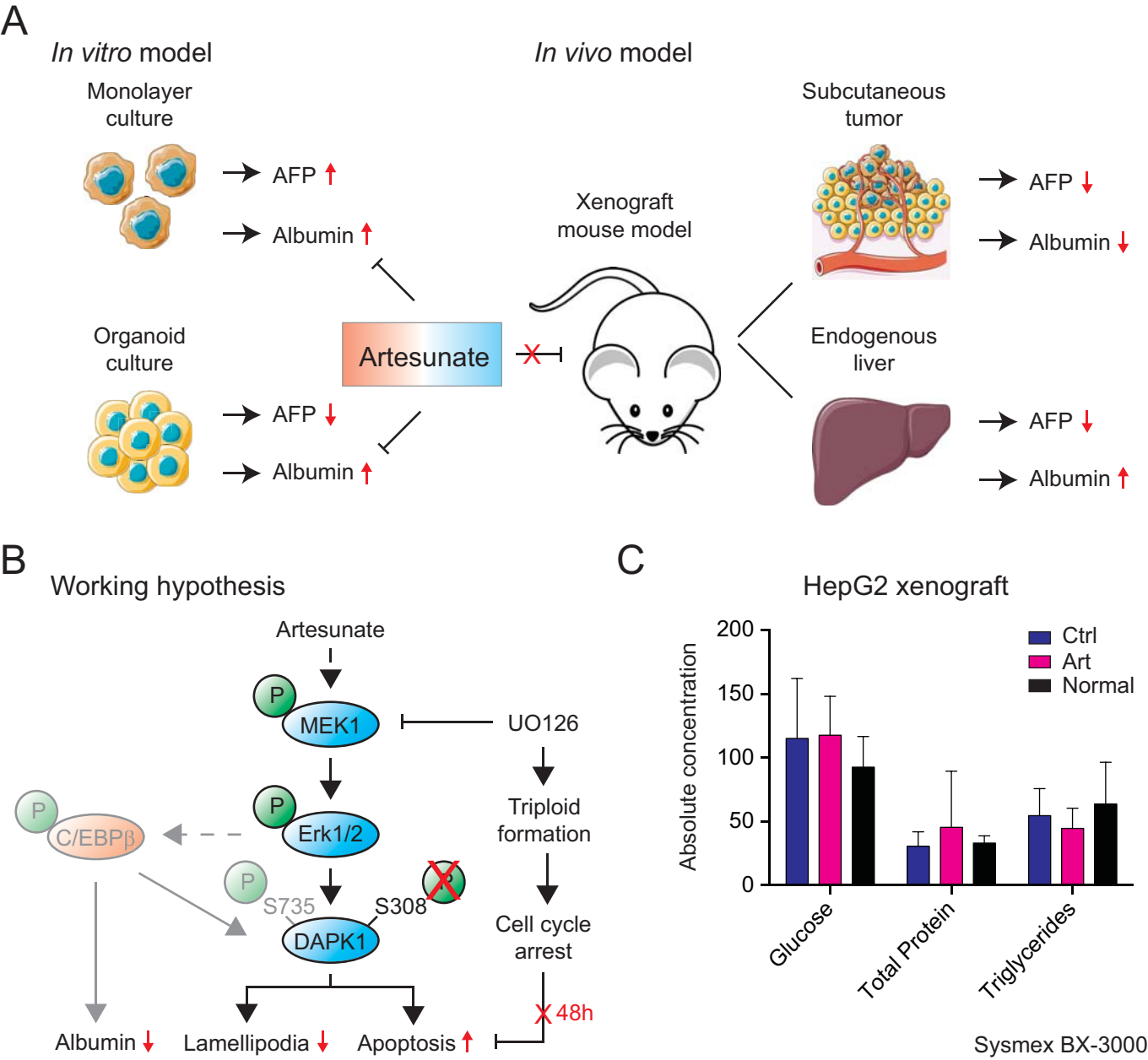
A
In vitro model
In vivo model
Monolayer culture
AFP ↑
Albumin ↑
Organoid culture
AFP ↓
Albumin ↑
Artesunate
Xenograft mouse model
Subcutaneous tumor
AFP ↓
Albumin ↓
Endogenous liver
AFP ↓
Albumin ↑
B
Working hypothesis
Artesunate
P
MEK1
UO126
Triploid formation
P
Erk1/2
P
C/EBPβ
P
S735
S308
DAPK1
Cell cycle arrest
48h
Albumin ↓
Lamellipodia ↓
Apoptosis ↑
C
HepG2 xenograft
Absolute concentration
200
150
100
50
0
Ctrl
Art
Normal
Glucose
Total Protein
Triglycerides
Sysmex BX-3000